Chinese Chemical Letters 33 (2022) 3435–3438

Contents lists available at ScienceDirect

Chinese Chemical Letters

journal homepage: www.elsevier.com/locate/cclet

Fluorination reaction of UO_3 and electrochemical preparation of UO_2

Rugeng Liu, Yangyang Meng, Wenjing Ji, Wei Han*, Mei Li*, Yang Sun

Key Laboratory of Superlight Materials and Surface Technology, Ministry of Education, College of Material Science and Chemical Engineering, Harbin Engineering University, Harbin 150001, China

ARTICLE INFO

Article history:
Received 27 December 2021
Revised 25 February 2022
Accepted 25 February 2022
Available online 1 March 2022

Keywords:
UO_3
Fluorination reaction
NH_4HF_2
Electrochemical formation
UO_2

ABSTRACT

In this work, a technique was proposed to prepare UO_2 from UO_3 by the two processes of fluorination reaction of UO_3 with NH_4HF_2 and electrochemical reduction of UO_2^{2+} for the recycle uranium. The feasibility of fluorination reaction was firstly confirmed using thermodynamic calculation; then, the products were analyzed using XRD, Raman and fluorescence to be UO_2F_2. The fluorination mechanism was inferred to be $UO_3(s)+NH_4HF_2 \rightarrow (NH_4)_3UO_2F_5 \rightarrow NH_4(UO_2)_2F_5 \rightarrow UO_2F_2$. The redox behavior of UO_2^{2+} on W electrode was investigated by cyclic voltammetry and square wave voltammetry, which indicated that UO_2^{2+} was reduced to UO_2 *via* a two-step single electron transfer with diffusion-controlled. The diffusion coefficient of UO_2^{2+} was calculated to be 6.22×10^{-5} cm^2/s. The disproportionation reaction of UO_2^{+} was observed, and the relationship between the disproportionation reaction and scan rate was discussed. Moreover, the electrochemical fabrication of UO_2 was conducted by electrolysis at −0.8 V, and the product was analyzed by XRD, SEM and EDS to be UO_2. ICP-AES results showed that the extraction efficiency of UO_2 could reach 98.53%.

© 2022 Published by Elsevier B.V. on behalf of Chinese Chemical Society and Institute of Materia Medica, Chinese Academy of Medical Sciences.

The reprocessing of spent fuel is one of the critical steps in the nuclear fuel cycle. In recent decades, extensive studies have been carried out on dry reprocessing using molten salt as a medium [1–3]. Thereinto, the electrolytic refining process developed by the United States and oxide-electrowinning reprocessing developed by Russia as are considered as the prominent candidate technologies for advanced nuclear fuel reprocessing in the future [4,5]. For MOX spent fuel, removing the cladding material is an important step in head-end process of spent fuel reprocessing. Recently, high temperature oxidation technology was adopted to separate spent fuel from cladding material by high temperature calcination UO_2 to form a volume expansion force to destroy the cladding material, which was proposed by Idaho national laboratory (TNL) and Korea atomic energy research institute (KAERI). During the process, UO_2 is oxidized to U_3O_8 and UO_3 [6]. In the oxide-electrowinning process, uranium and fission products in the oxide fuel are firstly chlorinated and dissolved into the molten salt as oxychloride (uranyl ion) and chloride ions by flowing chlorine gas, then uranyl ion is reduced to form the raw material of MOX fuel (UO_2) on the cathode in molten chlorides. However, the spontaneity of the chlorination reaction is unfavorable, and hence, it is necessary to add reducing agents, for instance, carbon and carbon monoxide into the melts [7]. Thus, many investigators explored the chlorination reaction of uranium oxide (UO_2 and U_3O_8) using $ZrCl_4$ [8], CCl_4 [9,10], NH_4Cl [11]. Sakamura *et al.* [8] studied UO_2 was chlorinated to form UCl_4 by $ZrCl_4$ in LiCl-KCl melt, however, the conversion rate was only 37%. Kitawaki *et al.* [9] explored the chlorination UO_2 and U_3O_8 using CCl_4 through mechanical mixing method, but did not succeed. Jiang *et al.* [10] chlorinated U_3O_8 to UCl_4 using CCl_4 at high temperature, but CCl_4 would volatilize severely and the by-product of UCl_5 was formed. As we known, UCl_5 is easy to volatilize which causes the loss of uranium. Liu *et al.* [11] investigated the chlorination reaction of U_3O_8 and NH_4Cl in LiCl-KCl melt under air atmosphere. Their results showed that U_3O_8 can be successfully chlorinated to UO_2^{2+}. Wani *et al.* [12] studied the fluorination of UO_2 and U_3O_8 with NH_4HF_2 and found the formation of $[NH_4]_4UF_8$ and $[NH_4]_3UO_2F_5$ compounds. These two compounds, on heating to about 673 K could form UF_4 and $UO_2F_2{\cdot}2H_2O$, respectively.

The electrochemical reduction of UO_2^{2+} has been explored in molten chlorides and found that UO_2^{2+} can be reduced to UO_2 by two-step single electron transfer [13–16]. Schlechteret *et al.* [17] reported that the crystalline form of electrodeposited UO_2 in LiCl-KCl molten salt was affected by the presence of fluoride, and the presence of a small amount of fluoride would be conducive to the formation of cubic crystal UO_2. Caligara *et al.* [18] measured the diffusion coefficient of UO_2^{2+} in molten LiCl-KCl eutectic.

In order to explore the route of the formation of UO_2 using UO_3 as raw material, NH_4HF_2 was chosen as fluoride reagent to

* Corresponding authors.
E-mail addresses: weihan@hrbeu.edu.cn (W. Han), meili@hrbeu.edu.cn (M. Li).

https://doi.org/10.1016/j.cclet.2022.02.069
1001-8417/© 2022 Published by Elsevier B.V. on behalf of Chinese Chemical Society and Institute of Materia Medica, Chinese Academy of Medical Sciences.

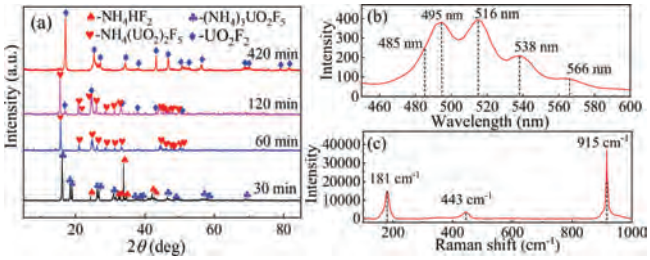

Fig. 1. (a) XRD patterns of products obtained at 573 K for 30 min, 60 min, 120 min, 420 min. (b) Fluorescence spectrum and (c) Raman spectrum.

make uranium oxide change to UO_2^{2+} under air atmosphere. Then, the electrochemical formation of UO_2 was investigated in LiCl-KCl molten salt by constant potential electrolysis for uranium extraction. The fluoride product and electrodeposition sample were checked by XRD, SEM-EDS.

Firstly, the possibility of the formation of UO_2F_2 from UO_3 was estimated using the thermodynamic analysis of related fluorination reactions. UO_3 can react with NH_4HF_2 or HF obtained from the decomposition of NH_4HF_2 to form UO_2F_2, the following reactions may be involved as follows:

$$3UO_3(s) + 6NH_4HF_2(s) = 3UO_2F_2(s) + 6NH_4F + 3H_2O(g) \quad (1)$$

$$3UO_3(s) + 6NH_4HF_2(s) = 3UO_2F_2(s) + 6NH_3(g) + 6HF(g) + 3H_2O(g) \quad (2)$$

$$UO_3(s) + 2HF(g) = UO_2F_2(s) + 3H_2O(g) \quad (3)$$

The standard Gibbs free energy changes ($\Delta_r G_m^{\ominus}$) for these reactions at various temperatures were calculated shown in Fig. S1 (Supporting information). It can be seen that ($\Delta_r G_m^{\ominus}$) of these reactions are less than zero, which means that all the reactions correlated with the formation of UO_2F_2 are spontaneous at the temperature of 473–873 K. Moreover, the ($\Delta_r G_m^{\ominus}$) becomes more and more negative with the increasing temperature, indicating that the increase of temperature can be beneficial to the fluorination reaction of UO_3.

The fluorination reaction of UO_3 with NH_4HF_2 was performed at 573 K for different times. The obtained products were characterized by XRD shown in Fig. 1a. It can be seen from Fig. 1a that after the fluorination reaction for 30 min, only $(NH_4)_3UO_2F_5$ is observed except for the unreacted NH_4HF_2. No diffraction peak of UO_3 occurs, indicating that UO_3 is firstly converted to $(NH_4)_3UO_2F_5$. After 60 min, only $NH_4(UO_2)_2F_5$ appears, which shows that $(NH_4)_3UO_2F_5$ is completely converted to $NH_4(UO_2)_2F_5$. When the fluorination reaction time is extended to 120 min, the diffraction peak of UO_2F_2 is observed. However, $NH_4(UO_2)_2F_5$ is not completely decomposed, and its diffraction peaks can still be observed. However, after the reaction for 420 min, XRD result indicates there are only UO_2F_2, and $NH_4(UO_2)_2F_5$ has been completely converted to UO_2F_2.

To further confirm the formation of UO_2F_2, fluorescence spectroscopy and Raman spectroscopy were used to analyze the product obtained from the fluorination of UO_3 for 180 min at 673 K. It can be seen from Fig. 1b that peaks maxima appear at about 485, 495, 516, 538 and 566 ± 0.5 nm, showing a five-finger shape, which is a typical characteristic peak of UO_2^{2+} [19,20]. Fig. 1c shows the Raman spectrum of the product. Three obvious vibration peaks are observed at 181 cm^{-1}, 443 cm^{-1} and 915 cm^{-1}, respectively. Among them, the strong band at 915 cm^{-1} is ascribed to the symmetric U-O stretching vibration. The band at 181 cm^{-1} corresponds to the U-O bending fundamental and the weaker band at 443 cm^{-1}

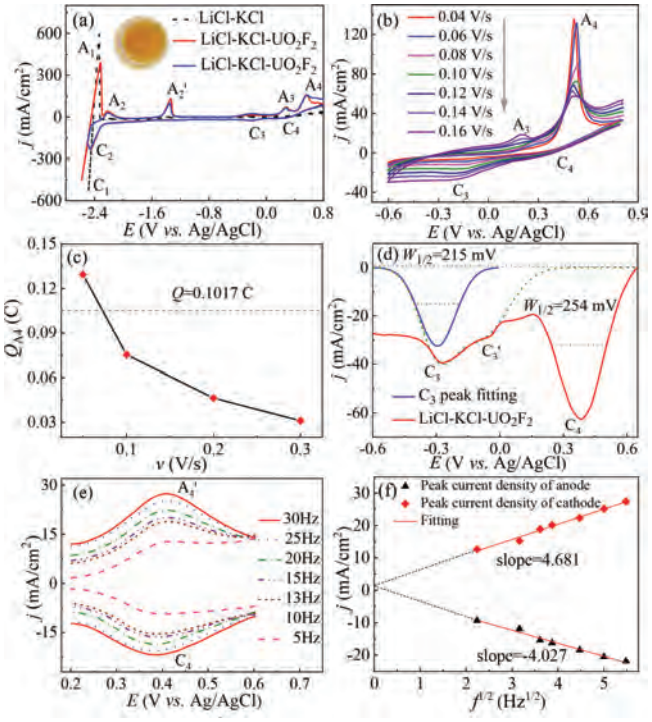

Fig. 2. CV curves of UO_2^{2+} at (a) 0.1 V/s and (b) various scan speed. (c) The relationship of electricity amount and scan speed. (d) SWV curve of UO_2^{2+} at 20 Hz. (e) Various frequencies, and (f) fitting line of peak current density versus square root of frequency ($f^{1/2}$).

is related to the U-F lattice vibration which are consistent with those of UO_2F_2 obtained by Armstrong *et al.* [21]. These results demonstrate the formation of UO_2F_2.

The reaction mechanism is expressed as follows:

$$UO_3(s) + 3NH_4HF_2(s) = (NH_4)_3UO_2F_5(s) + H_2O(g) + HF(g) \quad (4)$$

$$2(NH_4)_3UO_2F_5(s) = NH_4(UO_2)_2F_5(s) + 5NH_3(g) + 5HF(g) \quad (5)$$

$$NH_4(UO_2)_2F_5(s) = 2UO_2F_2(s) + NH_3(g) + HF(g) \quad (6)$$

The products obtained under different fluorination times at 573 K were analyzed by SEM to observe the morphology changes. Fig. S2 (Supporting information) shows the SEM images of fluorination products obtained at different duration. It can be seen that UO_3 presents a spherical particle with size of about 1 μm. UO_3 was fluorinated for 30 min, according to the XRD result, $(NH_4)_3UO_2F_5$ with size of about 3 μm is formed. A truncated octahedral composed of four hexagons and ten quadrilaterals is observed in Fig. S2b. After 60 min of the reaction, according to the XRD result, $(NH_4)_3UO_2F_5$ is decomposed to $NH_4(UO_2)_2F_5$, and NH_3 and HF are released. Thus, a small number of pores are observed on the surface of the particles (Fig. S2c). When the reaction proceeds for 420 min, the product is UO_2F_2 based on the XRD result. It can be observed from Fig. S2d that the formation of pores appears on the surface of the particles due to the release of NH_3 and HF, which indicates that large amounts of NH_3 and HF have been released.

Then the electrode reaction of UO_2^{2+} was studied in LiCl-KCl melts on Mo electrode at 773 K using cyclic voltammetry (CV) shown in Fig. 2a. In the black line, peaks C_1 and A_1 are attributed to the deposition and dissolution of metallic Li. While UO_2^{2+} was added into LiCl-KCl melts, the color of the molten salt change from colorless to yellow shown in the inset of Fig. 2a, which is exactly the color of UO_2^{2+} dissolved in molten salt. In the red line, four new anodic peaks, A_2, A_2', A_3 and A_4, are observed at −2.21 V, −1.42 V, 0.27 V and 0.54 V, respectively. Only three cathodic peaks, C_2, C_3

and C_4, are observed at −2.45 V, −0.31 V and 0.32 V, respectively. The redox couple C_4/A_4 may be correlated with the soluble/soluble redox process of UO_2^{2+}/UO_2^{+}.

$$UO_2^{2+} + e^- \leftrightarrow UO_2^{+} \quad (7)$$

The C_3/A_3 couple pertains to the formation of UO_2 and its re-oxidation.

$$UO_2^{+} + e^- \leftrightarrow UO_2 \quad (8)$$

The C_2/A_2 couple is ascribed to the reduction of UO_2 to U metal and oxidation of U metal, and A_2' corresponds to the dissolution of U to U^{3+} [22,23].

Fig. 2b presents the CV curves of LiCl-KCl-UO_2^{2+} (0.24 wt%) melts at various scan speeds. For the redox peaks of C_3/A_3, with the increase of the scan rate, the cathodic/anodic peak currents increase and the cathodic/anodic peak potentials have a significant negative/positive shift which shows that the Eq. 9 is not a reversible process. However, for the redox peaks of C_4/A_4, with the increase of the scan rate, the cathodic peak current increases and anodic peak current decreases. It can be seen that when the scan rate is 0.04 V/s and 0.06 V/s, the oxidation peak A_3 is not observed. A_4 is related to the UO_2^{+} to disproportionate into UO_2 (monolayer) and it has a sharp shape and a large peak current. When the scan rate reaches 0.08 V/s, peak A_3 appears, and the peak current of A_4 decreases rapidly, the peak potential shifts negatively, and the peak become widens. When the scan rate increases from 0.1 V/s to 0.16 V/s, the peak current of A_3 continued to increase, the peak current of A_4 gradually decreases, and peak A_4 became wider.

This phenomenon may be caused by the disproportionation reaction of UO_2^{+}.

$$2UO_2^{+} \leftrightarrow UO_2^{2+} + UO_2 \quad (9)$$

At low scan rate, the measurement time is relatively long, the formed UO_2^{+} has enough time to generate UO_2^{2+} and UO_2 by the disproportionation Eq. 9, and the concentration of UO_2^{+} decreases, which results in that the current peaks C_3 and A_3 related to the reduction and oxidation of UO_2^{+} are not obvious. As the scan rate increases, the disproportionation reaction time is reduced, and the amount of UO_2 generated by the disproportionation reaction gradually decreases, the peak current of the oxidation peak A_4 gradually decrease and oxidation peak A_3 gradually appears.

The electrode area is 0.3768 cm^2. Assuming that a layer of UO_2 was deposited on the electrode surface, the electric quantity of A_4 which was integrated of the peak area required by disproportionation reaction is at least 0.102 C. To obtain the electric quantity passed during oxidation reaction, the current and oxidation time related to the peak A_4 in Fig. 2b was integrated, and then the relationship of quantity of electricity versus scan rate was plotted, as shown in Fig. 2c. It can be seen that when the scan rate is relatively low, the electric quantity passing through the oxidation peak A_4 is close to that required to theoretically deposit a single layer of UO_2. As the scan rate increases, the electric quantity passing through peak A_4 gradually decreases, which meant the amount of UO_2 deposited at A_4 gradually decreases. This is consistent with the analysis result in Fig. 2b and further proves that the existence of oxidation peak A_4 is correlated with the formation of UO_2 by the disproportionation reaction of UO_2^{+}.

To further illustrating the electrochemical reactions correlated with peaks C_3 and C_4, the square wave voltammetry (SWV) was used to measure the number of electron-transferred during the two electrochemical reactions. Fig. 2d shows the SWV curve when reduction reaction of UO_2^{2+} occurs on W electrode. In the measured potential range, three reduction peaks (C_3, C_3' and C_4) are observed and then the number of electrons transferred obtained by Eq. 10.

$$W_{1/2} = 3.52RT/nF \quad (10)$$

where $W_{1/2}$ is the half-peak width; R is ideal gas constant; T is absolute temperature; F is Faraday constant; and n is the number of electrons transferred.

Since the appearance of peak C_3', which may be related to the nucleation of UO_2 [24], will interfere with the calculation result peak C_3, the Gaussian fitting was performed to eliminate the influence. Using Eq. 10, the number of electron transfer attributed to the peak C_3 is 1.09, close to 1. Thus, the reaction correlated with peak C_3 is the reduction reaction of UO_2^{+} to UO_2 *via* a one-step involving one electron.

And the calculated number of electron-transferred from the reduction peak of C_4 is 0.92, close to 1, which means the reaction pertaining to peak C_4 is that UO_2^{2+} is reduced to UO_2^{+} in a one-step with the exchange of one-electron. Fig. 2d shows the SWV curves of LiCl-KCl-UO_2F_2 melts at various frequencies. As shown in Fig. 2e, a pair of obvious redox peaks A_4'/C_4 appears at around −0.40 V, and their shape is flat and symmetrical, which indicates that the redox reaction is a reversible reaction in a soluble/soluble system. Plotting the peak current density and the square root of the frequency, a good linear relationship indicates that the redox reaction is controlled by diffusion (Fig. 2f). Thus, the diffusion coefficient of UO_2^{2+} can be calculated using Eq. 11 [25].

$$J_{pc} = nFC_0\frac{1-\sigma}{1+\sigma}\sqrt{\frac{Df}{\pi}},\ \sigma = \exp\left(\frac{nF}{RT}\cdot\frac{E_{SW}}{2}\right) \quad (11)$$

where C_0 is concentration of UO_2^{2+} in the molten salt ($C_0 = 9.804\times10^{-5}$ mol/cm^3); D is diffusion coefficient (cm^2/s); n is numbers of electrons transfer ($n = 1$); f is frequency; E_{SW} is amplitude of SWV ($E_{SW} = 0.1$ V).

The calculated diffusion coefficient of UO_2^{2+} at 773 K is 6.22×10^{-5} cm^2/s, which has the same order of magnitude with the literature (1.54×10^{-5} cm^2/s) obtained on platinum electrode at 858 K [18].

According to the electrochemical results, it is feasible for the formation of UO_2 by molten electrolysis. Thus, potentiostatic electrolysis was performed to form UO_2 at −0.8 V for 8 h. The change of current with time was recorded, as shown in Fig. 3a. A strong current appears at the beginning (inset), which might be related to the formation and growth of UO_2 nuclei. Before 1500 s, the current fluctuated at −20 mA, meaning the formation of UO_2. However, with the proceeding, the concentration of UO_2^{2+} decreases, leading to the decrease of the absolute value of current. When the *I-t* curve became steady and close to background current about 2 mA, it could be considered that the run is completed.

The XRD spectra of the product gained shown in Fig. 3b indicates the formation of UO_2 successfully and the color of the Mo plate changes from metallic luster to black, as shown in inset of Fig. 3b. After stripping off the UO_2 from the electrode, the diffraction peaks in XRD spectra shown in Fig. 3b became stronger and sharper, showing the deposited UO_2 has a high crystallinity. The morphology and element distribution were characterized, as shown in Figs. 3c-f, the UO_2 is unevenly distributed on the electrode surface in a dendritic state. EDS analysis also proved the formation of UO_2. Before and after the run, the concentration of U in the melts was analyzed by ICP-AES and the extraction efficiency was calculated using Eq. 12. The calculated result indicated that after 8 h electrolysis, the extraction of UO_2 can reach 98.53%.

$$\eta = \frac{C_1 - C_2}{C_1}\times 100\% \quad (12)$$

where η is extraction efficiency; C_1 and C_2 are the initial and final concentrations of UO_2^{2+} in the melts, respectively.

In order to electrochemically form UO_2 using UO_3 as raw material, the formation of UO_2F_2 by the fluorination reaction of UO_3 and NH_4HF_2 and its mechanism were firstly studied using XRD, Raman and fluorescence. The results revealed the for-

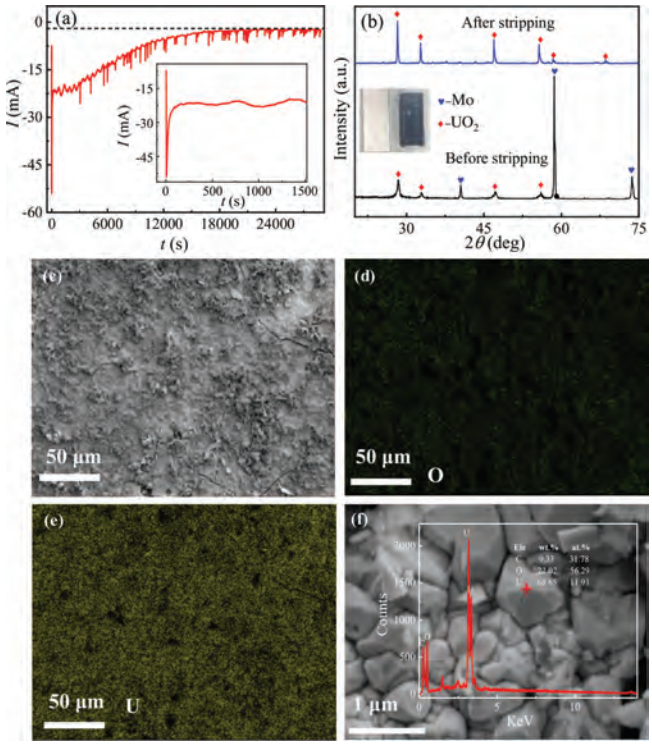

Fig. 3. (a) *I-t* curve, (b) XRD patterns and (c) SEM-EDS images of electrolysis product obtained by potentiostatic electrolysis at −0.8 V on Mo plate at 773 K.

mation of UO_2F_2, and the mechanism was inferred to be comprised of the following three process $UO_3(s) + 3NH_4HF_2(s) \rightarrow (NH_4)_3UO_2F_5 \rightarrow NH_4(UO_2)_2F_5(s) \rightarrow 2UO_2F_5(s)$. Then, the electrochemical formation of UO_2 was studied using CV and SWV, which illustrated UO_2^{2+} could be reduced to UO_2 *via* a two-step single electron exchange process with diffusion-controlled. The diffusion coefficient of UO_2^{2+} was estimated to be 6.22×10^{-5} cm^2/s. The disproportionation reaction of UO_2^{+} was observed, and the relationship between the disproportionation reaction and scan rate was discussed. In addition, UO_2 was prepared employing potentiostatic electrolysis at −0.8 V for 8 h in LiCl-KCl-UO_2F_2 melt. XRD and SEM-EDS results indicated UO_2 with micron-sized octahedral structure was formed, and the extraction efficiency of UO_2 calculated by ICP-AES could reach 98.53%. The feasibility of UO_2 prepared using UO_3 as raw material was proved.

Declaration of competing interest

The authors declare that they have no known competing financial interests or personal relationships that could have appeared to influence the work reported in this paper.

Acknowledgments

The work was financially supported by the National Natural Science foundation of China (Nos. U2167215, 22076035, 21876034, 11875116 and 21790373), and the Fundamental Research Funds for the Central Universities (No. 3072021CFJ1001).

Supplementary materials

Supplementary material associated with this article can be found, in the online version, at doi:10.1016/j.cclet.2022.02.069.

References

[1] D.W. Yang, Y.L. Liu, T.Q. Yin, et al., Electrochim. Acta 353 (2020) 136449.
[2] Y.K. Zhong, Y.L. Liu, K. Liu, et al., Nat. Commun. 12 (2021) 5777.
[3] D.W. Yang, S.L. Jiang, Y.L. Liu, et al., Sep. Purif. Technol. 281 (2022) 119853.
[4] S. Vavilov, T. Kobayashi, M. Myochin, J. Nucl. Sci. Technol. 41 (2004) 1018–1025.
[5] J.L. Willit, W.E. Miller, J.E. Battles, J. Nucl. Mater. 195 (1992) 229–249.
[6] B.R. Westphal, J.J. Park, J.M. Shin, et al., Sep. Sci. Technol. 43 (2008) 2695–2708.
[7] Y.S. Yang, Y.H. Kang, H.K. Lee, Mater. Chem. Phys. 50 (1997) 243–247.
[8] Y. Sakamura, T. Inoue. T. Iwai, H. Moriyama, J. Nucl. Mater. 340 (2005) 39–51.
[9] S. Kitawaki, T. Nagai, N. Sato, J. Nucl. Mater. 439 (2013) 212–216.
[10] K. Jiang, V. Smolenski, A. Novoselova, et al., Electrochim. Acta 318 (2019) 194–201.
[11] Y.C. Liu, Y.L. Liu, L. Wang, et al., J. Nucl. Mater. 542 (2020) 152475.
[12] B.N. Wani, S.J. Patwe, U.R. Rao, K.S. Venkateswarlu, J. Fluorine Chem. 44 (1989) 177–185.
[13] J.R. Chalkley, J. Less Common Met. 3 (1961) 98–109.
[14] T. Nagai, T. Fujii, O. Shirai, H. Yamana, J. Nucl. Sci. Tech. 41 (2004) 690–695.
[15] T. Nagai, A. Uehara, T. Fujii, O. Shiral, H. Yamana, J. Nucl. Sci. Tech. 43 (2006) 1511–1516.
[16] I. Uchida, J. Niikura, S. Toshima, J. Electroanal. Chem. 124 (1981) 165–177.
[17] M. Schlechter, J. Kooi, R. Billiau, R.A. Charlier, G.L. Dumont, J. Nucl. Mater. 15 (1965) 189–200.
[18] F. Caligara, L. Martinot, G. Duyckaerts, J. Electroanal. Chem. 16 (1968) 335–340.
[19] J.Y. Lee, J.Y. Oh, K. Putri, M. Baik, J.I. Yun, J. Radioanal. Nucl. Chem. 312 (2017) 221–231.
[20] Y. Sihn, J.I. Yun, W. Lee, J. Radioanal, Nucl. Chem. 308 (2016) 413–423.
[21] D.P. Armstrong, R.J. Jarabek, W.H. Fletcher, Appl. Spectrosc. 43 (1989) 461–467.
[22] Y.K. Zhong, K. Liu, Y.L. Liu, et al., J. Electrochem. Soc. 166 (2019) D276–D282.
[23] H.M. Li, R.G. Liu, W. Han, et al., Electrochimi. Acta 400 (2021) 139474.
[24] D. Han, C. She, J. Peng, et al., J. Electrochem. Soc. 165 (2018) 301–306.
[25] E.P. Parry, R.A. Osteryoung, Anal. Chem. 37 (1965) 1634–1637.